Solvent-switchable continuous breathing behaviour in a diamondoid metal-organic framework and its influence on CO_2 vs CH_4 selectivity

Elliot J. Carrington[1], Craig A. McAnally[2], Ashleigh J. Fletcher[2], Stephen P. Thompson[3], Mark Warren[3] and Lee Brammer[1,*]

[1]Department of Chemistry, University of Sheffield, Brook Hill, Sheffield S3 7HF

[2]Department of Chemical and Process Engineering, University of Strathclyde, 75 Montrose Street, Glasgow, G1 1XJ

[3]Diamond Light Source, Harwell Science and Innovation Campus, Didcot, Oxon, OX11 0DE

Abstract

Understanding the behaviour of flexible metal–organic frameworks (MOFs)—porous crystalline materials that undergo a structural change upon exposure to an external stimulus—underpins their design as responsive materials for specific applications, such as gas separation, molecular sensing, catalysis and drug delivery. Reversible transformations of a MOF between open- and closed-pore forms—a behaviour known as 'breathing'—typically occur through well-defined crystallographic transitions. By contrast, continuous breathing is rare, and detailed characterization has remained very limited. Here we report a continuous-breathing mechanism that was studied by single-crystal diffraction in a MOF with a diamondoid network, (Me2NH2)[In(ABDC)2] (ABDC, 2-aminobenzene-1,4-dicarboxylate). Desolvation of the MOF in two different solvents leads to two polymorphic activated forms with very different pore openings, markedly different gas adsorption capacities and different CO2 versus CH4 selectivities. Partial desolvation introduces a gating pressure associated with CO2 adsorption, which shows that the framework can also undergo a combination of stepped and continuous breathing.

Metal-organic frameworks (MOFs) are a structurally and compositionally varied class of porous materials that are the subject of intensive investigation of their host-guest behaviour for various applications including molecular sensing, drug delivery, catalysis and gas or liquid separations.[1-7] Among MOFs that permit reversible guest removal and uptake, most have a rigid pore structure reminiscent of harder inorganic porous materials such as zeolites. A recent estimate indicates that only around 100 out of some 20,000 reported MOFs exhibit breathing or flexible behaviour in response to external stimuli.[8] Such MOFs present opportunities for improved performance in applications that take advantage of selective adsorption properties.[8-10] The dynamic behaviour of these materials can occur through a variety of mechanisms including a rotation of the organic linkers, a hinge motion of the carboxylate groups that commonly connect ligands to the metal nodes or a displacement of subnetworks relative to each other.[11-13] These motions lead to opening or closing of pores and are associated with loss/uptake of guest molecules. The structural changes occur predominantly through defined transitions between different crystalline states, a process commonly referred to as "breathing."[11,14-17] This behaviour results in stepped adsorption isotherms, which may exhibit a hysteresis that can be exploited in gas capture or separation applications.[18-20] The most well-studied MOFs that exhibit such defined transitions are those with a pillared or columnar structure that contain 1D channels with a diamond or square cross-section, which compress or expand upon breathing in

a manner analogous to that of a wine-rack. Such MOFs include the paddlewheel MOF DMOF,[21-23] [Zn$_2$(BDC)$_2$(dabco)] (BDC = 1,4-benzenedicarboxylate or derivatives; dabco = 1,4-diazabicyclooctane) and azolate MOFs [M(BDP)] (M = Fe, Co; BDP = 1,4-benzenedipyrazolate).[18,24] The archetype of such materials is the MIL-53 family of MOFs ([M(X)[BDC] (M = trivalent Al, Cr, Fe, Ga; X = OH, F), which exhibit defined phase transitions between wide-pore (wp) and a narrow-pore (np) forms, upon desolvation and gas uptake.[14,15,20,25-27]

MOFs that exhibit large flexibility, but without defined transitions, are much rarer and are not well understood. The prototypical example of such *continuous* breathing behaviour, often referred to as "swelling," is the MIL-88 family of MOFs, which undergo very large changes in pore size on solvation/desolvation. These structural changes could be quantitatively modelled only by a combined computational and powder X-ray diffraction (PXRD) approach.[28,29] The studies indicated that, like the MIL-53 materials, a hinge motion, associated with the carboxylate coordination, is the dominant component of the flexible behaviour, an aspect we will examine later in this article. The challenge of structural characterisation of breathing MOFs is a pervasive one and, for example, materials that are amenable to the most accurate characterisation by single crystal diffraction throughout their dynamic behaviour are uncommon, but highly sought after.[30-32]

Here we report a new example of continuous breathing behaviour in the MOF (Me$_2$NH$_2$)[In(ABDC)$_2$] (**SHF-61**) (ABDC = 2-aminoterephthalate; SHF = Sheffield Framework), for which full characterization by both single crystal and powder X-ray diffraction offers unusually detailed structural insight into the flexibility. Originally reported as a static MOF with high CO$_2$/CH$_4$ selectivity,[33] we reveal that this MOF exhibits a large breathing behaviour, with a mechanism that differs from that of previously reported flexible MOFs. **SHF-61** is a 3-dimensional diamondoid MOF constructed from In^{3+} ions chelated by four 2-aminoterephthalate (ABDC) ligands resulting in a flattened tetrahedral network geometry at the indium centres. The material exhibits remarkable sensitivity to the nature of the guest solvent, such that activation by removal of different solvent guests leads to dramatic differences in gas adsorption capacity and in CO$_2$ vs CH$_4$ selectivity. Partial desolvation of the MOF introduces a gating mechanism and stepped isotherm for the adsorption of CO$_2$, which is absent in the fully activated (desolvated) material.

Results and Discussion

Synthesis and crystal structure. Metal-organic framework compound **SHF-61** was synthesised by solvothermal reaction of InCl$_3$ with 2-aminoterephthalic acid in DMF.[33] The as-synthesised material, **SHF-61-DMF**, comprises a doubly-interpenetrated anionic diamondoid framework with pores containing dimethylammonium cations generated *in situ* from hydrolysis of DMF. The solvent content was established by combination of elemental analysis and TGA to give the formula (Me$_2$NH$_2$)[In(ABDC)$_2$]·1.75DMF·1.25H$_2$O. Solvent within the pores was also exchanged for CHCl$_3$ by soaking **SHF-61-DMF** in dry CHCl$_3$ to give **SHF-61-CHCl$_3$**. The MOF was characterised by ^{13}C CP-MAS NMR spectroscopy and both single crystal and powder X-ray diffraction, the latter confirming phase purity. The framework structure (Figure 1) is almost identical for both solvated forms, **SHF-61-DMF** and **SHF-61-CHCl$_3$**. Amino substituents on the terephthalate ligand are ordered, in contrast to the typical site-disorder observed for ABDC ligands in other MOFs.[34,35] Ordering is consistent with the prominent role of the amino groups in linking the two networks via a 4-membered hydrogen-bonded ring motif (Figure 1c). The framework exhibits lozenge-shaped channels that lie along the *a*-axis, resembling those of aforementioned flexible MOFs such as MIL-53, although there is no pillar along the channel direction, but rather a helical arrangement of In(III) centres linked via ABDC ligands (Figure 1d).
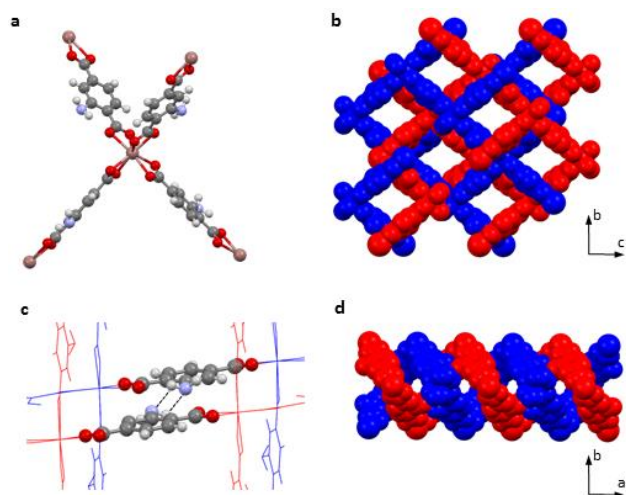
Figure 1 | Crystal structure of SHF-61. a, In$(O_2CR)_4$ tetrahedral network node. **b**, View down *a*-axis showing lozenge-shaped channels. **c**, Hydrogen-bonding interaction between amino groups of adjacent networks. **d**, View down *c*-axis showing helical arrangement of the two interpenetrated networks along the channel axis (*a*-axis).

Gas adsorption and selectivity. Activation of **SHF-61-DMF** and **SHF-61-CHCl₃** was examined by TGA measurements. Both show two distinct mass losses prior to full thermal decomposition of the framework, consistent with removal of solvent followed by Me_2NH from the cations. The onset of mass loss associated with the cation occurs at 500 K for **SHF-61-DMF** but at only 390 K for **SHF-61-CHCl₃**. Samples were, therefore, activated under vacuum at 423 K and 353 K, respectively, conditions designed to remove the solvent but retain the $Me_2NH_2^+$ cations. Mass losses on activation correspond well to those expected for solvent removal. Solid-state ^{13}C NMR and IR spectroscopy confirmed complete removal of DMF from **SHF-61-DMF** (see Supplementary Figure 3).

The activation routes from **SHF-61-DMF** and **SHF-61-CHCl₃** lead to very different gas adsorption behaviour (Figure 2) of the resultant framework **SHF-61**. **SHF-61-CHCl₃**, upon activation, exhibits type I adsorption isotherms[36] for N_2 (77 K, Langmuir surface area 544 $m^2\ g^{-1}$) and CO_2 (298 K, max.: 6.25 mmol g^{-1} at 19.5 bar), consistent with previously reported measurements.[33] Uptake of CH_4 (298 K) also follows a type I isotherm with maximum uptake of 2.6 mmol g^{-1} at 4.5 bar (*cf.* 4.45 mmol g^{-1} CO_2 at 4.5 bar), in contradiction to the previously reported absence of CH_4 uptake to pressures of 30 bar.[33] We determined, however, that the equilibration times for the CH_4 measurements were long (3-6 h per mass point) suggesting that the excellent separation of CO_2 vs. CH_4 in the previously reported breakthrough experiments[33] is a consequence of the large difference in adsorption kinetics between CO_2 and CH_4. Uptake for all three gases was substantially lower for the directly-activated **SHF-61-DMF** than its counterpart **SHF-61-CHCl₃**. Almost negligible adsorption for N_2 at 77 K (BET surface area 2.93 $m^2\ g^{-1}$) was observed, and only a modest uptake for CO_2 (298 K, max.: 1.46 mmol g^{-1} 4.5 bar, 2.43 mmol g^{-1} 18 bar) and CH_4 (298 K, max.: 1.47 mmol g^{-1} 4.5 bar). These changes in adsorption behaviour result in a change in selectivity, wherein activation from **SHF-61-CHCl₃** gives rise to a material that is selective for CO_2 over CH_4, whereas direct activation of **SHF-61-DMF** results in no selectivity between these gases.

The adsorption behaviour of activated **SHF-61-CHCl₃** is consistent with a Langmuir adsorption model,[37] whereas that for activated **SHF-61-DMF** conforms to the BET model[38] (see Supplementary Information sections 3.1 and 3.2). The Langmuir model suggests monolayer formation with CO_2 molecules primarily occupying the walls of the pore, whereas a BET model suggests multilayer formation, with a narrower pore-shape that encourages interaction between multiple CO_2 molecules across the pore. The isosteric heat of adsorption (Q_{st}) at zero coverage determined for the MOF activated directly from **SHF-61-DMF** (22 kJ mol^{-1}, see Supplementary Information section 3.1) also differs from that reported after activation following $CHCl_3$ (35.8 kJ mol^{-1}).[33] The differences in the isotherms suggest a significant

difference in the pore structure of **SHF-61** when generated by activation from **SHF-61-DMF** and **SHF-61-CHCl₃**, respectively. This prompted us to undertake a detailed crystallographic examination of the framework structure during desolvation and gas adsorption.
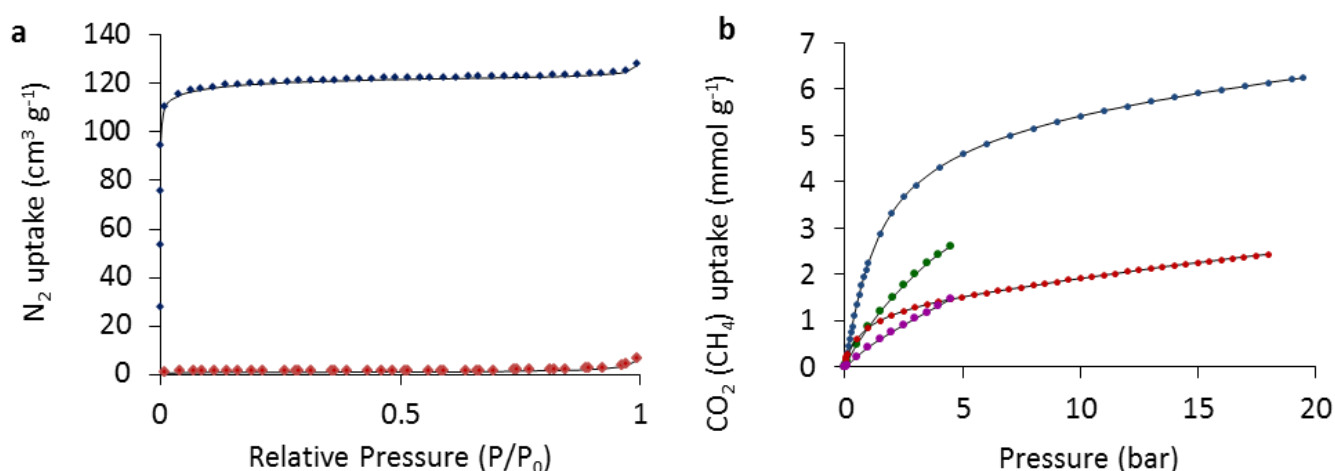
Figure 2 | Gas adsorption by SHF-61. a, Volumetric N_2 adsorption isotherms at 77 K following activation from **SHF-61-DMF** (red circles CO_2) and from **SHF-61-CHCl₃** (blue circles CO_2). **b**, Gravimetric adsorption isotherms at 298 K following activation from **SHF-61-DMF** (red circles CO_2, purple circles CH_4) and from **SHF-61-CHCl₃** (blue circles CO_2, green circles CH_4).

Reversible and solvent-dependent continuous breathing behaviour. A series of crystal structure determinations of **SHF-61-DMF**, desolvated to different extents by heating for different periods of time or at different temperatures, revealed a large breathing motion associated with the removal of the DMF and water molecules (Figure 3). This motion is not associated with a defined phase transition but rather is a *continuous* change, an effect which so far has only been reported for the MIL-88 MOFs to our knowledge. The structural changes are most evident in the crystallographic *b*- and *c*-axis directions where correlated contraction ($\Delta b \approx 6$ Å) and elongation ($\Delta c \approx 4$ Å) is observed over the range of the continuous breathing motion, resulting in narrowing of the lozenge-shaped channels upon solvent loss (Figure 3a). Although this appears to resemble the behaviour of 'wine-rack' MOFs such as MIL-53 and DMOF, the overall behaviour in **SHF-61** is dissimilar as a result of its different network connectivity and topology. Thus, **SHF-61** is not rigid along the channel direction, and undergoes a smaller continuous reduction in length of the *a*-axis ($\Delta a \approx 0.45$ Å), associated with a compression of the helices shown in Figure 1d, which cannot occur in wine-rack MOFs. The full range of motion results in a large change in unit cell volume ($\Delta V \approx 2000$ Å³, ~15%) but no change in symmetry. The breathing is also evident macroscopically, resulting in a marked change in dimensions and morphology of the single crystals upon desolvation (Figure 3a). Analogous studies of microcrystalline **SHF-61-DMF** by PXRD confirm the breathing behaviour in the bulk material (see Supplementary Information section 2.5).

The breathing mechanism is enabled by two principal deformations of the framework. There is a hinge motion that involves rotation of the ABDC ligands about the O···O vector of each carboxylate group. This is accompanied by a change in the coordination geometry at the In(III) centres, which results in a flattening of the tetrahedral arrangement that defines the network topology. No discernible subnetwork displacements are evident. Comparison of the two deformation components with those of other well-studied breathing MOFs indicates that the change in coordination angle ($\Delta\gamma$ in Figure 3b) is a more important contributor to the breathing mechanism in **SHF-61** than in MIL-53, MIL-88 and DMOF, for which the ligand hinge motion ($\Delta\theta$) accounts for almost all of the breathing behaviour.
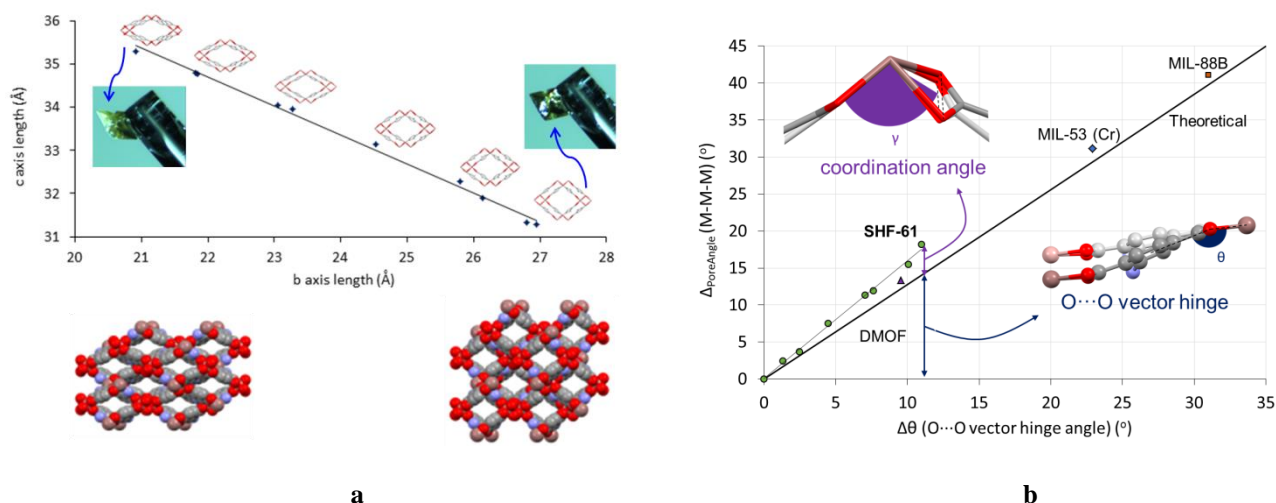
Figure 3 | Continuous breathing of SHF-61 on desolvation and comparison to other breathing MOFs. a, Changes to the *b*- and *c*-axis lengths of **SHF-61-DMF** during solvent removal. Each data point represents a low temperature single crystal structure (100-120 K) obtained after a crystal was heated at a different temperature or for a different period of time. The pore geometry viewed down the *a*-axis is shown for each structure. Cations and solvent molecules are not shown. Spacefilling representations showing a larger section of the structure at the wide pore and narrow pore extremes are shown below and changes to the morphology and macroscopic dimensions of the crystal are shown as insets. **b**, The principal contributions to the pore (angle) deformation that results from breathing behaviour is shown for **SHF-61** in comparison to DMOF, MIL-53 and MIL-88. Pore angle change (vertical axis) is approximately the sum of the change in coordination angle at the metal centre(s) and the hinge motion associated with rotation of the ligand about the carboxylate O···O vector. The theoretical line defines the pore angle change associated only with the hinge motion contribution. For all definitions and full analysis see Supplementary Information section 5.

Given that activation of the two solvated forms of **SHF-61** led to very different gas adsorption behaviour, single crystal and powder X-ray diffraction studies during desolvation of **SHF-61-CHCl₃** were also conducted (Supplementary information sections 2.6 and 4.1). Desolvation of **SHF-61-CHCl₃** results in the same type of continuous breathing effect, but of a much smaller magnitude ($\Delta b \approx -0.6$ Å; $\Delta c \approx 0.6$ Å), than observed for **SHF-61-DMF**, although with a similarly small compression of the helices along the pore direction ($\Delta a \approx -0.4$ Å). Thus, the crystal structure of **SHF-61** is confirmed as existing in two different desolvated (activated) forms, a narrow-pore form when activated from **SHF-61-DMF** and a wide-pore form when activated from **SHF-61-CHCl₃**. These can be considered to be polymorphs of **SHF-61**, which correlate with the highly dissimilar gas uptakes in the corresponding adsorption measurements.

Reversibility of the continuous breathing deformation was confirmed by permitting uptake of water vapour from air by a sample of **SHF-61-DMF**, after desolvation *in situ* by heating at 423 K under N_2. Two *in situ* PXRD experiments were conducted on microcrystalline samples in capillaries. The first sample was exposed to air following partial desolvation to an intermediate level of pore opening ($a = 15.217(2)$, $b = 23.827(4)$, $c = 33.60(1)$ Å). Unit cell dimensions obtained from Pawley fitting[39] of powder patterns (30 min intervals) change in accord with the continuous breathing mechanism, following the reverse of the DMF desolvation pathway (Figure 4) and leading to a wide-pore structure after 12 h ($a = 15.3497(7)$, $b = 25.954(2)$, $c = 32.068(3)$ Å). An analogous sample was heated at 423 K under N_2 in a Schlenk tube and transferred to a capillary in an Ar-filled glovebox to prevent any exposure to air. This led to greater desolvation and closure of the pores ($a = 15.004(3)$, $b = 21.764(6)$, $c = 34.838(9)$ Å). Upon cutting open the end of the sealed capillary, powder patterns were measured at intervals over a period of 42 d as the framework adsorbed water vapour and returned to a wide-pore (fully solvated) form ($a = 15.40(1)$, $b = 26.01(2)$, $c = 31.94(3)$ Å) (full details in Supplementary Information section 2.7). The markedly slower opening rate of the pores during water uptake, when the starting point is a more closed structure, further implicates guest-framework interactions in having a prominent role in the breathing mechanism.
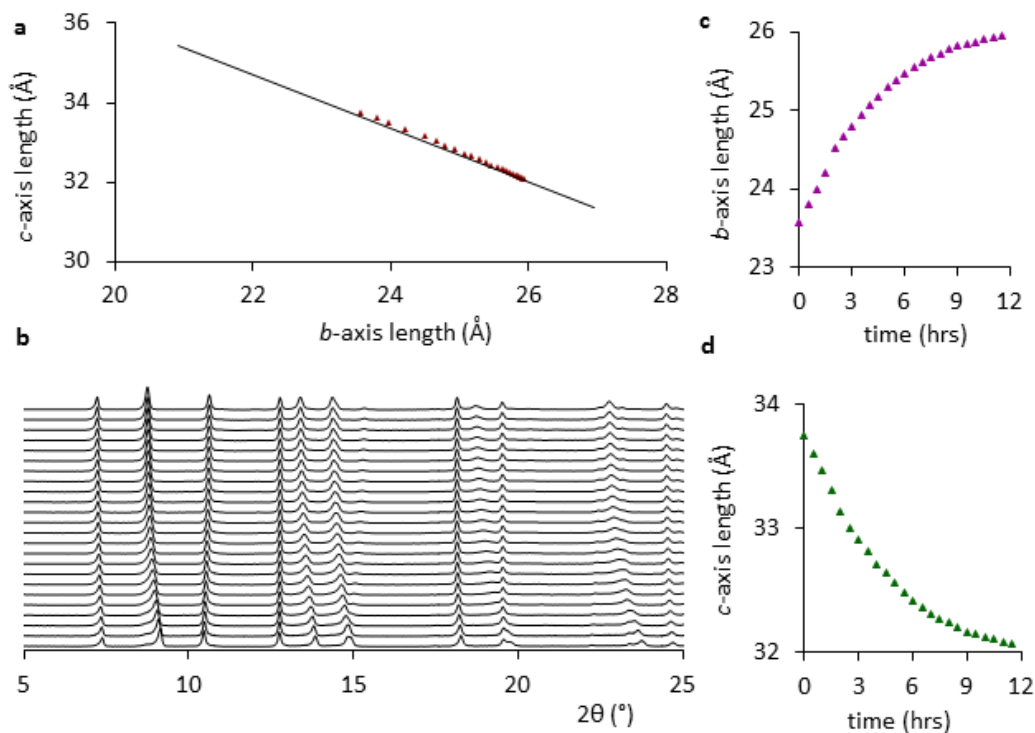
Figure 4 | Continuous breathing of SHF-61 on resolvation. a, Changes to the *b*- and *c*-axis lengths of partially desolvated **SHF-61-DMF** during atmospheric water uptake. Each data point has been obtained from Pawley refinement of a powder pattern. The trendline shown is that drawn for the *ex situ* desolvation represented in Figure 3a. **b**, Powder patterns recorded every 30 min on a laboratory instrument during the uptake of atmospheric water vapour. **c**, Evolution of the *b*-axis length with time. **d**, Evolution of the *c*-axis length with time.

Induced gating of CO_2 adsorption by partial framework desolvation. Gas adsorption behaviour in partially desolvated MOFs is typically not investigated as the focus is often on uptake capacity, which requires study of the fully desolvated MOF (*vide supra*). As part of our investigation of the newly discovered flexible behaviour, however, we have conducted both *in situ* PXRD during CO_2 adsorption and a gravimetric CO_2 adsorption study, in both cases starting from the as-synthesised **SHF-61-DMF** with approximately one-third of the solvent content removed (Figure 5). To our knowledge this is the first example of such a study in a MOF. Remarkably, the partially solvated MOF exhibits a stepped CO_2 adsorption isotherm, in contrast to the type I isotherms observed for the fully desolvated MOF after either DMF/H_2O or $CHCl_3$ removal. An initial rapid uptake of CO_2 (≤ 0.5 mmol g^{-1}) is followed by a slow increase and, upon exceeding a gate pressure (~7 bar), the material undergoes a further rapid uptake of CO_2. On reducing the CO_2 pressure, hysteresis is observed, accompanied by a similar step in the isotherm. The maximum uptake of CO_2 at 20 bar is 2.4 mmol g^{-1}, approximately one-third of the maximum uptake observed for the wide-pore framework after full desolvation from **SHF-61-CHCl₃**, indicating that the pore-space is two-thirds filled by DMF/H_2O and one-third filled by CO_2. The stepped isotherm now resembles that observed for the MIL-53 family and other well-known breathing MOFs, and suggests a structural phase transition which triggers the second rapid uptake of CO_2. *In situ* PXRD studies during CO_2 uptake identify the structural change in the same narrow pressure range as the step in the gravimetric adsorption isotherm. This change corresponds to a sudden opening of the pores of the framework from a partially closed structure (associated with the initial partially desolvated state) to a wide-pore structure. The framework, however, is not in a fixed state at either side of the transition and undergoes a small, gradual pore expansion with increasing gas pressure both before and after the transition. On reducing the pressure, the framework closes in a similar manner to its opening. There is initially a small, gradual closure of the pores, followed by a sudden larger closure, and then a further small, gradual closure at the lowest pressures. The structural changes exhibit a hysteresis with pressure that corresponds well to that observed in the gravimetric adsorption measurements.
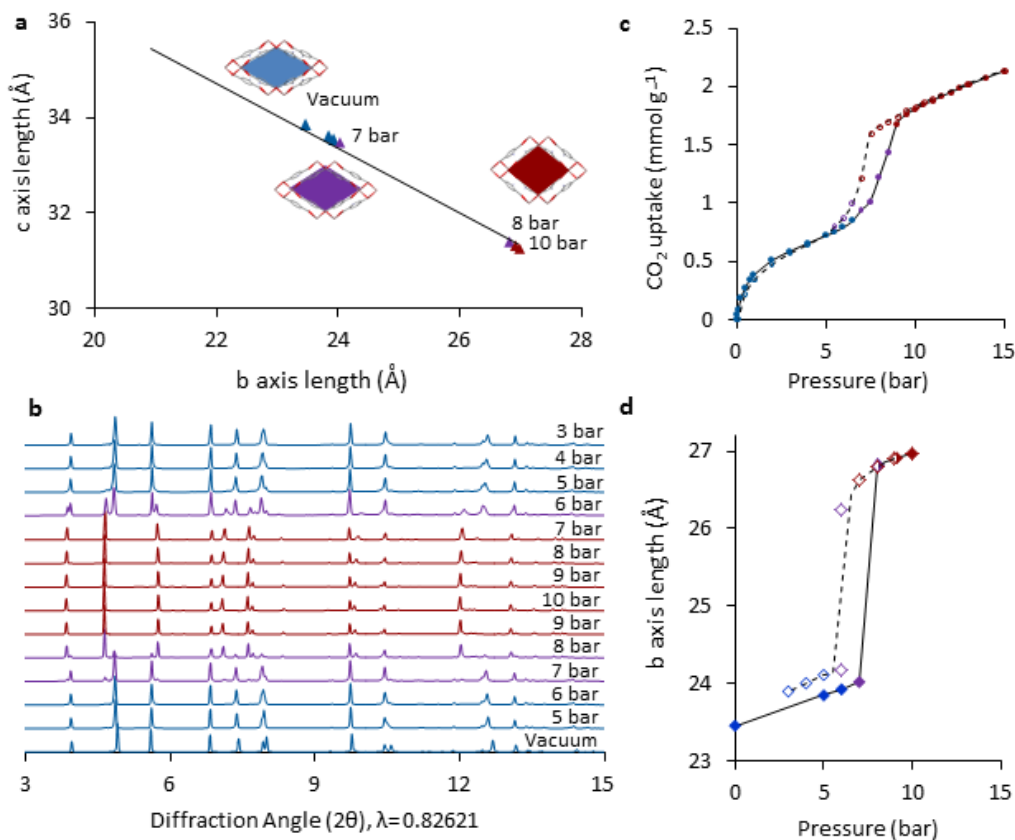
Figure 5 | Gated CO₂ uptake by partially-solvated SHF-61-DMF. *In situ* powder diffraction studies during CO₂ uptake (at 298 K) by a partially closed (partially desolvated) sample of **SHF-61-DMF**. **a**, b- and c-axis unit cell values from Pawley refinements of powder patterns of partially-solvated **SHF-61-DMF** upon increasing CO₂ pressure (points associated with reducing CO₂ pressure not shown for clarity). **b**, Powder diffraction patterns at evolving CO₂ pressures. **c**, Gravimetric CO₂ adsorption isotherm at 298 K for **SHF-61-DMF** containing 68% of the solvent present in its as-synthesised form. **d**, CO₂ pressure vs b-axis length showing structural change and hysteresis consistent with gravimetric CO₂ adsorption data. All plots are colour-coded: blue is partially closed framework, red is open framework and purple is the intermediate region in which the transition takes place.

Guest-framework interactions and the breathing mechanism. Although only limited information on cation and guest locations within the MOF pores could be established from the crystallographic studies, the crystallographic models of the framework's flexible behaviour, coupled with the gas adsorption measurements, strongly implicate guest-framework and cation-framework interactions in controlling the framework breathing behaviour (Figure 6). The clearest evidence comes from the difference in breathing behaviour during desolvation of the as-synthesised form (containing DMF and H₂O) compared with the CHCl₃-exchanged form. Both adopt almost identical framework structures when solvent-filled, but the former undergoes gradual pore closure through a continuum of structures during solvent loss, leading to a desolvated narrow-pore structure, whereas the latter undergoes only approximately 10% of the pore closure on full desolvation. DMF and H₂O molecules are anticipated to have attractive intermolecular interactions with the framework and cation that are stronger than those for CHCl₃, in particular via hydrogen bonding or other electrostatic interactions. Thus, it is suggested that the gradually diminishing quantity of DMF/H₂O molecules help to maintain interactions across the pores that favour pore closure enabled by the breathing of the framework, resulting ultimately in a solvent-free framework that is maintained in a narrow-pore form by cation-framework interactions. This process is reversible on uptake of water vapour. The much weaker interactions formed by CHCl₃ molecules with both framework and cation do not enable substantial pore closing and, importantly, loss of all CHCl₃ does not lead to cation-mediated pore closure. This contrasts with the behaviour of the MIL-53 MOFs, which transform from open to closed form instantaneously due to a strong bridging interaction across the closed pores provided by inclusion of a

small amount of water (or even CO_2). There is precedence for a MOF exhibiting both wide- and narrow-pore solvent-free forms. MIL-53(Fe) and MIL-53(Cr) exist in closed and open desolvated forms, respectively, but neither has been shown to adopt both desolvated forms.[40] [Al(OH)(ndc)] (ndc = 2,6-napthalenedicarboxylate) can be synthesised as a narrow-pore form (as MIL-69) and wide-pore form as DUT-4,[41] resembling the extremes of the breathing motions of MIL-53, but unlike **SHF-61** these MOFs have been shown to be neither flexible nor interconvertible.
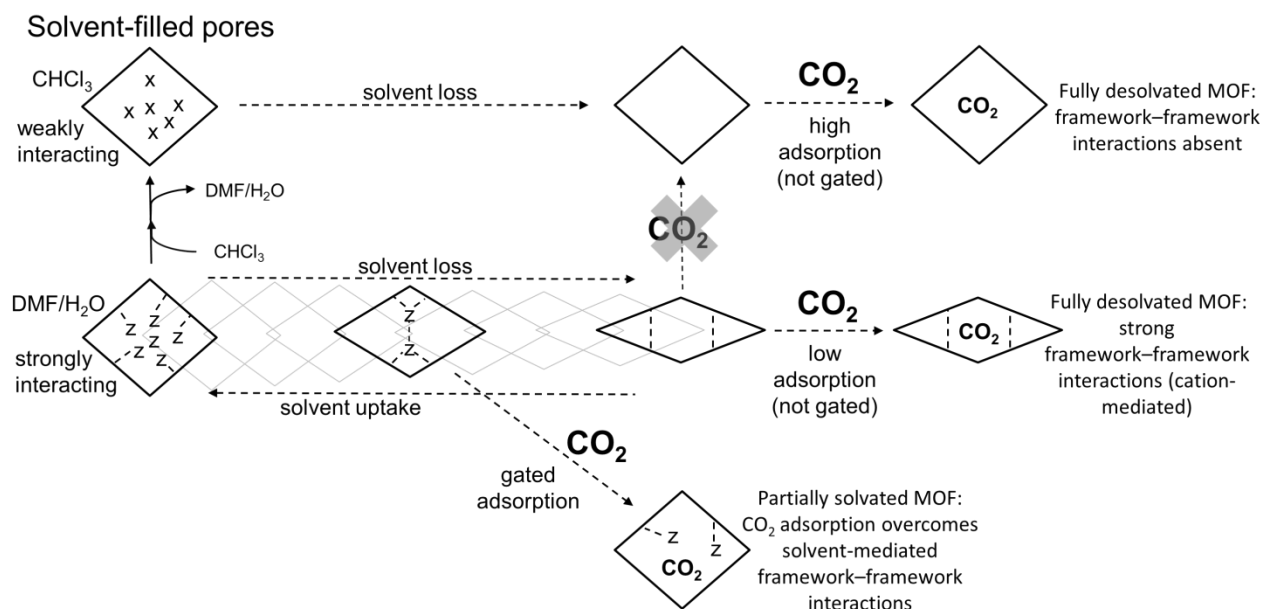
Figure 6 | Proposed role of guest-framework interactions in the solvent-dependent continuous breathing properties of SHF-61. The MOF is represented schematically by diamond-shaped quadrilaterals analogous to the pore cross-section when viewed down the *a*-axis of the crystal structure. Solvent molecules within the pores are represented by symbols **X** ($CHCl_3$) or **Z** (DMF/H_2O). Dashed lines represent stronger intermolecular interactions within the pores. **SHF-61-DMF** reversibly loses and adsorbs solvent vapour accompanied by a continuous breathing of the MOF pores, due to strong solvent-framework interactions, whereas **SHF-61-CHCl₃** loses solvent without substantial change in pore dimensions, due to weak solvent-framework interactions. The two desolvated forms (wide-pore from $CHCl_3$-activation and narrow-pore from DMF-activation) exhibit markedly different CO_2 uptake capacities (also observed for CH_4 and N_2 uptake). Partial desolvation of **SHF-61-DMF** enables *gated* CO_2 adsorption, leading to full opening of the pores, as CO_2 is now able at modest pressures to overcome framework-solvent and other interactions that prevent the framework from fully opening. This contrasts with the adsorption of CO_2 in the narrow-pore framework obtained after complete activation of **SHF-61-DMF**, for which CO_2 adsorption does not lead to pore opening, presumably due to strong (cation-mediated) framework-framework interactions.

It is anticipated that CO_2 will be a more weakly interacting guest than DMF or water but more strongly interacting than $CHCl_3$. This is consistent with the framework breathing behaviour observed upon CO_2 uptake. The most closed form of the MOF, following desolvation from **SHF-61-DMF**, has a modest CO_2 uptake at 298 K and follows a type I adsorption isotherm typical of a fixed pore size. Thus, the CO_2-framework interactions are too weak to overcome the stronger cation-framework interactions that maintain the most closed form. This assertion is confirmed by comparable results obtained on repeating the adsorption measurement at 258 K in order to reach relative pressure of $P/P_0 \approx 0.84$ at 20 bar CO_2 (*cf.* $P/P_0 \approx 0.3$ at 298 K). The partially desolvated **SHF-61-DMF**, however, takes up CO_2 initially, resulting in a small expansion of the pores, which is then followed by a sudden opening of the pores at 7-8 bar, coinciding with a step in the adsorption isotherm, before continuing with a small final pore expansion. This suggests that the presence of some solvent in the pores enables CO_2, once reaching a gate pressure, to force open the pores. Crystallographic studies during CH_4 adsorption using partially desolvated **SHF-61-DMF**, result in only a small (continuous) expansion of the MOF pores, suggesting that interactions of CH_4 with the framework are too weak to fully overcome framework-solvent interactions (see Supplementary Information section 4.3).

Conclusions

Although MOFs with indium tetracarboxylate nodes are well-established, the only reports of framework flexibility involve either specific ligand flexibility[42] or subnet rearrangements[43] rather than the mechanism reported herein. Our studies show that $(Me_2NH_2)[In(ABDC)_2]$ (**SHF-61**) displays a large amplitude *continuous* breathing behaviour which is distinct from that previously reported in other MOFs. Indeed, despite computational studies of known and hypothetical MOFs,[44] the breathing behaviour of this or similar MOFs has not been predicted to our knowledge. Continuous breathing, rather than defined structural transitions between open and closed forms, is extremely uncommon in MOFs, but for **SHF-61** can be studied crystallographically not only for powders but in single crystals, enabling remarkable structural and mechanistic insight. The breathing behaviour is highly guest-dependent and this dependence can be used to control gas uptake and selectivity between gases, notably CO_2 vs CH_4. The MOF can adopt either a narrow-pore or wide-pore form in its solvent-free state, these polymorphic forms arising from activation of the as-synthesised MOF **SHF-61-DMF** containing DMF/H_2O or the $CHCl_3$-exchanged MOF **SHF-61-CHCl₃**, respectively. The two activated forms of the MOF exhibit very different gas adsorption behaviour, with the wide-pore form leading to markedly greater uptake of CO_2, CH_4 and N_2, and introducing CO_2 vs CH_4 selectivity, thus enabling tuning of the adsorption properties by solvent-induced control of the breathing behaviour. Additionally it has been shown that a pressure-related gating of CO_2 adsorption effect is introduced if only partial desolvation of the MOF is undertaken. *In situ* crystallographic studies during CO_2 adsorption, considered alongside gravimetric CO_2 adsorption measurements, establish that the gating corresponds to a transition, which is absent in the gas adsorption by the fully desolvated forms, from a partially closed to an open-pore form. Despite the detailed experiments conducted in this study, however, a number of intriguing questions still remain and will be the subject of future studies. These include establishing whether the interpenetrated nature of the MOF, and the accompanying interframework interactions, play an important role in controlling the flexibility observed. Overall the discovery of this highly flexible breathing MOF provides considerable new insight into breathing behaviour and offers the potential to develop a new family of tunable, highly-responsive materials for which adsorption properties and other applications dependent on control of pore space can be exploited.

Methods

Synthesis of $(Me_2NH_2)[In(ABDC)_2]\cdot1.75DMF\cdot1.25H_2O$ (SHF-61-DMF). $InCl_3$ (0.1106 g 0.5 mmol) and 2-aminoterephthalic acid (0.092 g, 0.5 mmol) were dissolved in N,N-dimethylformamide (DMF) (10 mL), the resulting solution was then transferred to a 125 mL Teflon-lined steel autoclave and heated to 130 ^{o}C for 24 h. After cooling to room temperature the solvent was decanted off and the brown octahedron-shaped crystals were transferred and stored in fresh DMF (Yield: 46 %). Elemental analysis (% calc/found): C 41.70/41.69; H 4.93/4.93; N, 9.94/9.92.

Synthesis of $(Me_2NH_2)[In(ABDC)_2]\cdot n CHCl_3$ (SHF-61-CHCl₃). Single crystals of **SHF-61-DMF** were placed in dry $CHCl_3$ (1 mL), which was replaced daily for a minimum of 1 week.

Gravimetric gas adsorption in $(Me_2NH_2)[In(ABDC)_2]$ (SHF-61). Measurements were made using an Intelligent Gravimetric Analyser (*IGA*) supplied by Hiden Isochema Ltd, which was thermally regulated via active computer control. A computer algorithm was applied to monitor the approach to equilibrium at each pressure step. Prior to measurements, **SHF-61-DMF** was activated at 423 K under high vacuum and **SHF-61-CHCl₃** was activated at 353 K under high vacuum. The mass losses were monitored during the

process and correlated to those observed by thermogravimetric analysis. Measured mass losses are consistent with loss of only solvent. Partial desolvation experiments for **SHF-61-DMF** were carried out using a lower outgassing temperature to control the rate of desolvation, and manually interrupting the activation process when the required mass loss was achieved.

Single-crystal structure determination and refinement of SHF-61-DMF and SHF-61-CHCl₃ during desolvation. Single crystals of **SHF-61-DMF** or **SHF-61-CHCl₃** were removed from their solvent and dried by heating either *ex situ* using a temperature-controlled oven or *in situ* experiments using an Oxford Crystostream device on the diffractometer. X-ray diffraction data were collected on a Bruker SMART APEX-II CCD diffractometer operating a Mo-K$_\alpha$ sealed-tube X-ray source or a Bruker D8 Venture diffractometer equipped with a PHOTON 100 dual-CMOS chip detector and operating a Cu-K$_\alpha$ IµS microfocus X-ray source. Integrated intensity data were corrected for absorption using empirical methods based upon symmetry-equivalent reflections combined with measurements at different azimuthal angles.[45] All crystal structures were solved and refined against F^2 values. Full details are provided in the SI.

Crystallographic studies of water uptake by (Me₂NH₂)[In(ABDC)₂] (SHF-61). In two separate studies, powder samples of **SHF-61-DMF** were desolvated by heating under a flow of N₂ gas before being exposed to air and allowed to absorb water vapour. The unit cell parameters of the structure were monitored by powder X-ray diffraction during the uptake process. In study 1, a sample was packed into a 0.5 mm borosilicate capillary, with one end left open, and mounted on the Bruker D8 Advance diffractometer (Cu-K$_\alpha$ radiation). Using the co-axial nitrogen stream of the Cryostream device the sample was heated *in situ* to 423 K at 4 K/ min, maintained at 423 K for 20 min, and cooled to 298 K 4 K/min. A powder pattern was recorded under the nitrogen stream at 298 K. The nitrogen stream was removed to allow water uptake from the air and further patterns recorded during a 12-hour period. Pawley refinement[39] was used to determine the unit cell parameters during this process. The sequence of powder patterns is shown in Figure 4. A second sample of **SHF-61-DMF** was heated to 423 K, while located in a Schlenk tube under constant nitrogen flow, prior to loading into a 0.7 mm borosilicate capillary in an argon filled glovebox and flame-sealing the capillary immediately upon removal from the glovebox. This procedure avoided any exposure of the sample to atmospheric water vapour. Powder X-ray diffraction data were collected on a Bruker D8 diffractometer using Cu-K$_\alpha$ radiation at room temperature. After cutting open the end of the capillary tube, X-ray powder patterns were recorded periodically over a 42 d period in an analogous manner to the first study. The unit cell parameters of the obtained patterns were determined using Pawley refinements.[39] Full details of both studies are provided in the SI. Study 1 is illustrated in Figure 4.

Crystallographic studies of (Me₂NH₂)[In(ABDC)₂] (SHF-61) during gas sorption . Single crystal and powder X-ray diffraction experiments were carried out at beamlines I19[47] and I11,[48] respectively, at Diamond Light Source. The gas loading was precisely controlled and measured using an *in situ* gas-cell apparatus. Single crystal structures were solved and refined against F^2 values. All patterns were fitted by Pawley refinement[39] and some cases also by Rietveld refinement.[49] Full details are provided in the SI.

Data availability statement

Crystallographic data for the structures reported in this paper have been deposited at the Cambridge Crystallographic Data Centre, under the deposition numbers 1524325-1524343. Copies of these data can be obtained free of charge via www.ccdc.cam.ac.uk/data_request/cif. All other data supporting the findings of this study are available within the article and its Supplementary Information files, or from the corresponding author upon reasonable request. Supplementary Information files contain full details of syntheses, TGA measurements, single crystal and powder diffraction experiments, gas adsorption measurements and CP-MAS ¹³C NMR spectra.

References

1. Mueller, U. *et al.* Metal–organic frameworks—prospective industrial applications. *J. Mater. Chem.* **16**, 626-636 (2006).

2. Kreno, L. E. *et al.* Metal-organic framework materials as chemical sensors. *Chem. Rev.* **112**, 1105–1125 (2012).

3. Horcajada, P. *et al.* Metal-organic frameworks in biomedicine. *Chem. Rev.* **112**, 1232–1268 (2012).

4. Yoon, M., Srirambalaji, R. & Kim, K. Homochiral metal-organic frameworks for asymmetric heterogeneous catalysis. *Chem. Rev.* **112**, 1196–1231 (2012).

5. Sumida, K. *et al.* Carbon dioxide capture in metal-organic frameworks. *Chem. Rev.* **112**, 724–781 (2012).

6. Suh, M. P., Park, H. J., Prasad, T. K. & Lim, D.-W. Hydrogen storage in metal-organic frameworks. *Chem. Rev.* **112**, 782–835 (2012).

7. Carrington, E. C., Vitórica-Yrezábal, I. J. & Brammer, L. Crystallographic studies of gas sorption in metal–organic frameworks. *Acta Crystallogr.* **B70**, 404–422 (2014).

8. Schneemann, A. *et al.* Flexible metal–organic frameworks. *Chem. Soc. Rev.* **43**, 6062–6096 (2014).

9. Fletcher, A. J., Thomas, K. M. & Rosseinsky, M. J. Flexibility in metal-organic framework materials: Impact on sorption properties. *J. Solid State Chem.* **178**, 2491–2510 (2005).

10. Horcajada, P. *et al.* Flexible Porous Metal-Organic Frameworks for a Controlled Drug Delivery. *J. Am. Chem. Soc.* **130**, 6774–6780 (2008).

11. Férey, G. & Serre, C. Large breathing effects in three-dimensional porous hybrid matter: facts, analyses, rules and consequences. *Chem. Soc. Rev.* **38**, 1380–1399 (2009).

12. Murdock, C. R., Hughes, B. C., Lu, Z. & Jenkins, D. M. Approaches for synthesizing breathing MOFs by exploiting dimensional rigidity. *Coord. Chem. Rev.* **258-259**, 119–136 (2014).

13. Coudert, F.-X., Boutin, A., Jeffroy, M., Mellot-Draznieks, C. & Fuchs, A. H. Thermodynamic Methods and Models to Study Flexible Metal-Organic Frameworks. *ChemPhysChem* **12**, 247–258 (2011).

14. Serre, C. et al. Very Large Breathing Effect in the First Nanoporous Chromium(III)-Based Solids: MIL-53 or $Cr^{III}(OH) \cdot \{O_2C-C_6H_4-CO_2\} \cdot \{HOC-C_6H_4-CO_2H\}_x \cdot (H_2O)_y$. *J. Am. Chem. Soc.* **124**, 13519–13526 (2002).

15. Serre, C. *et al.* An Explanation for the Very Large Breathing Effect of a Metal–Organic Framework during CO_2 Adsorption. *Adv. Mater.* **19**, 2246–2251 (2007).

16. Xiao, J. *et al.* Crystalline structural intermediates of a breathing metal-organic framework that functions as a luminescent sensor and gas reservoir. *Chem. A Eur. J.* **19**, 1891–1895 (2013).

17. Coudert, F.-X., Mellot-Draznieks, C., Fuchs, A. H. & Boutin, A. Prediction of breathing and gate-opening transitions upon binary mixture adsorption in metal-organic frameworks. *J. Am. Chem. Soc.* **131**, 11329–11331 (2009).

18.   Salles, F. *et al.* Multistep N_2 Breathing in the Metal−Organic Framework Co(1,4-benzenedipyrazolate). *J. Am. Chem. Soc.* **132**, 13782–13788 (2010).

19.   Yang, W. *et al.* Selective CO_2 uptake and inverse CO_2/C_2H_2 selectivity in a dynamic bifunctional metal–organic framework. *Chem. Sci.* **3**, 2993-2999 (2012).

20.   Bourrelly, S. *et al.* Different adsorption behaviors of methane and carbon dioxide in the isotypic nanoporous metal terephthalates MIL-53 and MIL-47. *J. Am. Chem. Soc.* **127**, 13519–13521 (2005).

21.   Grosch, J. S. & Paesani, F. Molecular-level characterization of the breathing behavior of the jungle-gym-type DMOF-1 metal-organic framework. *J. Am. Chem. Soc.* **134**, 4207–4215 (2012).

22.   Wang, Z. & Cohen, S. M. Modulating Metal−Organic Frameworks To Breathe: A Postsynthetic Covalent Modification Approach. *J. Am. Chem. Soc.* **131**, 16675–16677 (2009).

23.   Henke, S., Schneemann, A., Wütscher, A. & Fischer, R. A. Directing the Breathing Behavior of Pillared-Layered Metal–Organic Frameworks via a Systematic Library of Functionalized Linkers Bearing Flexible Substituents. *J. Am. Chem. Soc.* **134**, 9464–9474 (2012).

24.   Mason, J. A. et al. Methane storage in flexible metal–organic frameworks with intrinsic thermal management. *Nature* **527**, 357–361 (2016).

25.   Loiseau, T. et al. A Rationale for the Large Breathing of the Porous Aluminum Terephthalate (MIL-53) Upon Hydration. *Chem. Eur. J.* **10**, 1373–1382 (2004).

26.   Llewellyn, P. L., Bourrelly, S., Serre, C., Filinchuk, Y. & Férey, G. How hydration drastically improves adsorption selectivity for CO_2 over CH_4 in the flexible chromium terephthalate MIL-53. *Angew. Chem. Int. Ed.* **45**, 7751–7754 (2006).

27.   Millange, F. et al. Effect of the nature of the metal on the breathing steps in MOFs with dynamic frameworks. *Chem. Commun.* 4732–4734 (2008).

28.   Mellot-Draznieks, C., Serre, C., Surblé, S., Audebrand, N. & Férey, G. Very Large Swelling in Hybrid Frameworks: A Combined Computational and Powder Diffraction Study. *J. Am. Chem. Soc.* **127**, 16273–16278 (2005).

29.   Serre, C. et al. Role of Solvent-Host Interactions That Lead to Very Large Swelling of Hybrid Frameworks. *Science* **315**, 1828–1831 (2007).

30.   Yang, C., Wang, X. & Omary, M. A. Crystallographic observation of dynamic gas adsorption sites and thermal expansion in a breathable fluorous metal-organic framework. *Angew. Chem. Int. Ed.* **48**, 2500–2505 (2009).

31.   Seo, J., Matsuda, R., Sakamoto, H., Bonneau, C. & Kitagawa, S. A Pillared-Layer Coordination Polymer with a Rotatable Pillar Acting as a Molecular Gate for Guest Molecules. *J. Am. Chem. Soc.* **131**, 12792–12800 (2009).

32.   Seo, J., Bonneau, C., Matsuda, R., Takata, M. & Kitagawa, S. Soft Secondary Building Unit: Dynamic Bond Rearrangement on Multinuclear Core of Porous Coordination Polymers in Gas Media. *J. Am. Chem. Soc.* **133**, 9005–9013 (2011).

33.   Yuan, B. et al. A microporous, moisture-stable, and amine-functionalized metal-organic framework for highly selective separation of CO_2 from CH_4. *Chem. Commun.* **48**, 1135–7 (2012).

34.   Eddaoudi, M. *et al.* Systematic design of pore size and functionality in isoreticular MOFs and their application in methane storage. *Science* **295**, 469–72 (2002).

35.   Mowat, J. P. S. *et al.* Structural Chemistry, Monoclinic-to-Orthorhombic Phase Transition, and CO_2 Adsorption Behavior of the Small Pore Scandium Terephthalate, $Sc_2(O_2CC_6H_4CO_2)_3$, and Its Nitro- And Amino-Functionalized Derivatives. *Inorg. Chem.* **50**, 10844–10858 (2011).

36.   Thommes, M., Kaneko, K., Neimark, A. V., Olivier, J. P., Rodriguez-Reinoso, F., Rouquerol, J. & Sing, K. S., Physisorption of gases, with special reference to the evaluation of surface area and pore size distribution (IUPAC Technical Report). Pure Appl. Chem. **87**, 1051-1069 (2015).

37.   Langmuir, I. The adsorption of gases on plane surfaces of glass, mica and platinum. *J. Am. Chem. Soc.* **40**, 1361–1403 (1918).

38.   Brunauer, S., Emmett, P. H. & Teller, E. Adsorption of Gases in Multimolecular Layers. *J. Am. Chem. Soc.* **60**, 309–319 (1938).

39.   Pawley, G. S. Unit-cell refinement from powder diffraction scans. *J. Appl. Cryst.* **14**, 357–361 (1981).

40.   Llewellyn, P. L. et al. Complex adsorption of short linear alkanes in the flexible metal-organic framework MIL-53(Fe). *J. Am. Chem. Soc.* **131**, 13002–13008 (2009).

41.   Senkovska, I. *et al.* New highly porous aluminium based metal-organic frameworks: Al(OH)(ndc) (ndc=2,6-naphthalenedicarboxylate) and Al(OH)(bpdc) (bpdc=4,4′-biphenyldicarboxylate). *Microporous Mesoporous Mater.* **122**, 93–98 (2009).

42.   Li, X. *et al.* The dynamic response of a flexible indium based metal–organic framework to gas sorption. *Chem.Commun.* **52**, 2277–2280 (2016).

43.   Yang, S. *et al.* A partially interpenetrated metal-organic framework for selective hysteretic sorption of carbon dioxide. *Nat. Mater.* **11,** 710–716 (2012).

44.   Sarkisov, L., Martin, R. L., Haranczyk, M. & Smit, B. On the Flexibility of Metal–Organic Frameworks. *J. Am. Chem. Soc.* **136**, 2228–2231 (2014).

45.   Sheldrick, G. M. *SADABS*, University of Göttingen, based on the method of Blessing[46]: Krause, L., Herbst-Irmer, R., Sheldrick, G. M. & Stalke, D. Comparison of silver and molybdenum microfocus X-ray sources for single-crystal structure determination. *J. Appl. Cryst.* **48**, 3–10 (2015).

46.   Blessing, R. H. An Empirical Correction for Absorption Anisotropy. *Acta Crystallogr.* **A51**, 33–38 (1995).

47.   Nowell, H., Barnett, S. A., Christensen, K. E., Teat, S. J. & Allan, D. R. I19, the small-molecule single-crystal diffraction beamline at Diamond Light Source. *J. Synchrotron Radiat.* **19**, 435–441 (2012).

48.   Thompson, S. P. *et al.* Fast X-ray powder diffraction on I11 at Diamond. *J. Synchrotron Radiat.* **18**, 637–648 (2011).

49.   Rietveld, H. M. A profile refinement method for nuclear and magnetic structures. *J. Appl. Cryst.* **2**, 65–71 (1969).

Acknowledgements

Author Contributions

L.B and E.J.C. conceived the project. E.J.C carried out syntheses and analysis of single crystal and powder X-ray diffraction data. C.A.M. and A.J.F. conducted gravimetric and volumetric gas adsorption measurements and analyses. M.W. and S.P.T. provided experimental set-ups and support for *in situ* synchrotron crystallographic measurements and data analysis. L.B. was responsible for the overall direction of the project. L.B. and E.J. C. prepared the manuscript and all other authors contributed to its discussion.

Competing financial interests

The authors declare no competing financial interests.

Table of Contents

Breathing metal–organic frameworks are attractive functional materials whose molecular-scale pores can reversibly open and close. In contrast to typical defined structural transitions, continuous breathing has now been observed for a diamondoid MOF. Removal of two different solvents leads to two desolvated polymorphs with dramatically different porosities and gas uptake properties, including CO_2/CH_4 selectivities. Partial desolvation introduces pressure-gated CO_2 adsorption.